CrystEngComm

Accepted Manuscript

ROYAL SOCIETY OF CHEMISTRY

www.rsc.org/crystengcomm

CrystEngComm

RSCPublishing

COMMUNICATION

Self-organizing Ge(111)/Al/glass structures through layer exchange in metal-induced crystallization

Cite this: DOI: 10.1039/x0xx00000x

K. Toko,*[a] K. Nakazawa,[a] N. Saitoh,[b] N. Yoshizawa,[b] and T. Suemasu[a]

Received ooth January 2014,
Accepted ooth January 2014

DOI: 10.1039/x0xx00000x

www.rsc.org/

We achieved the self-organization of Ge/Al/glass structures by using Al-induced layer exchange at 325 °C. Diffusion-limiting layers formed between Ge and Al significantly induced slow growth under thermal equilibrium conditions, and thus allowed for fabricating an energetically-stable (111)-oriented Ge layers with grains as large as 20 μm in size.

Germanium has been used in electronic optical devices such as photodiodes or tandem solar-cells because of its narrow band gap (0.66 eV) and large absorption coefficient (~10^4 cm^{-1} at 0.8 eV).[1,2] Moreover, (111)-oriented Ge acts as epitaxial templates for group III-V compound semiconductors, silicide materials, and aligned nanowires, used for light-emitting devices.[3–5] Thus, Ge-based photonic technology is a powerful candidate for advanced next-generation devices. The expensiveness of bulk-Ge substrates motivates researchers to substitute bulk-Ge substrates with Ge films on inexpensive glass (softening temperature: ~550 °C).[6] Fabricating large-grained polycrystalline Ge (poly-Ge) on glass at low temperatures has been investigated using solid-phase crystallization, sputtering, and chemical vapour deposition; however, the resulting Ge layers consist of small, submicron grains with random orientations.[7–9]

Al-induced crystallization (AIC), developed for fabricating polycrystalline Si on glass,[10–16] is a promising method for preparing large-grained Ge layers on glass at low temperatures.[17–25] In previous studies, we fabricated a large-grained, (111)-oriented Ge on glass via exchanges between Ge and Al layers, by controlling the annealing temperature and the thickness of Al and Ge layers.[26,27] Moreover, we promoted the growth in AIC by inserting a thin (~1 nm) Ge membrane below Al.[28] By combining this Ge insertion layer with a GeO_x interlayer, we lowered the crystallization temperature of a-Ge from 325 °C to 180 °C, an applicable temperature for flexible plastic substrates.[29]

Fabricating optical devices and characterizing its electrical properties both require a conducting layer under the semiconducting layer. To accomplish this, here we study inverted-AIC, beginning with an Al/amorphous Ge (a-Ge)/substrate structure, contrasting the a-Ge/Al/substrate structure used in normal AIC, as schematically shown in Fig. 1. By using inverted-AIC, we aim at the self-organization of a poly-Ge/Al/glass structure, i.e., the spontaneous formation of an Al lower electrode below the Ge layer, via the layer exchange between Ge and catalytic Al during annealing. Moreover, the inverted structure may allow us to suppress "hillocks" appearing the surface of normal AIC-Ge.[27] As revealed by the previous studies on Si, the growth parameters, such as, thickness, annealing temperature, and appropriate interlayer between Al and semiconductor layers, are different between normal and inverted structures.[30-33] Thus, this study investigates the inverted-AIC of a-Ge in detail. As a result, we achieve a large-grained (~20 μm), (111)-oriented Ge layer on an Al coated glass substrate.

In the experiments, three kinds of samples were prepared on SiO_2 glass substrates as summarized in Table I. The Ge and Al layers were deposited at room temperature by using RF magnetron sputtering with Ar plasma. The deposition rate was 23 nm/min for Ge and 25 nm/min for Al. The degree of purity for the sputtering targets was 99.99% for Ge and 99.9% for Al. Argon pressure during the sputtering was 0.2 Pa. The RF power was set to 100 W. Sample A is a normal AIC sample corresponding to Fig. 1(a), prepared to examine the effect of the inverted structure. This sample has a top a-Ge layer (60 nm) and a bottom Al layer (50 nm). In this study, Ge is slightly thicker than Al to obtain the good surface coverage of Ge on the substrate. The interlayer is a natively oxidized Al (AlO_x) membrane with a few nm thickness, formed by exposing Al to air for 10 min.[26,27]

Samples B and C are inverted-AIC samples corresponding to Fig. 1(b). These are prepared to obtain Ge/Al/glass structures, and are compared to optimize the interlayer between Ge and Al.

The two samples have a top Al layer (50 nm) and a bottom a-Ge layer (60 nm). Sample B has a natively oxidized Ge (GeO_x) interlayer formed by exposing Ge to air for 24 h. The thickness of the GeO_x is estimated to be about 1 nm according to the previous study.[34] Meanwhile, sample C has an AlO_x interlayer formed by exposing an Al layer (2 nm), prepared on Ge, to air for 10 min.

The samples were then annealed at a temperature of 325 °C in N_2 until layer exchanges were finished: 100 h for sample A, 1 h for sample B, and 15 h for sample C. Because Al reacts readily with O, there is the possibility of reducing GeO_x and forming AlO_x in sample B during annealing. However, a previous study on AIC-Ge using a GeO_x interlayer proved the presence of GeO_x interlayer even after layer exchange.[20] This result allows us to examine validly the effect of the interlayer material by comparing samples B and C.

The surface morphology of each sample was observed by using a scanning electron microscope (SEM) with an energy-dispersive x-ray spectrometer (EDX), where the electron acceleration voltage was 15 keV. The crystal quality was evaluated by using a micro-probe Raman scattering spectroscopy (spot size: 1 μm, wavelength: 532 nm) and a θ-2θ X-ray diffraction (XRD) measurement (spot size: 10 mm). The crystal orientations and the grain sizes of the resulting poly-Ge layers were characterized by electron backscatter diffraction (EBSD) analysis. Prior to the EBSD measurements, the surface of poly-Ge was cleaned using a diluted HF solution (1.5% HF) for 1 min. The cross-sectional structure and elemental composition were investigated by the analytical transmission electron microscope (TEM), FEI Tecnai Osiris operated at 200 kV, equipped with EDX and high-angle annular dark-field scanning transmission electron microscopy (HAADF-STEM) system with a probe diameter of ~1 nm. Cross-sectional TEM samples were prepared by conventional focused ion beam method.

Fig. 2 shows the surface morphologies of annealed samples evaluated by using SEM and EDX, indicating significantly different structures among the samples. For sample A, its surface consists of Al and Ge as shown in Fig. 2(a)–(c). This is a representative structure obtained by layer exchange in normal AIC: the sample has low-quality Ge hillocks stacked on a high-quality bottom-Ge layer.[27] For sample B, Fig. 2(d)–(f) show that Ge is present on the surface, demonstrating layer exchange between Al and Ge; however, the Ge layer is separated by Al and results in island shape. In contrast, for sample C, Fig. 2(g)–(i) show that Ge covers the entire region of the surface. The significant difference of the surface morphologies between samples B and C is discussed later. Note that strong Ge signals are partially visible in Fig. 2(e) and (h), corresponding to the bright areas in the SEM images shown in Fig. 2(d) and (g), respectively. The bright areas are not attributed to the outermost surface structures but to the inside structures, as determined by the following cross-sectional STEM-EDX analysis.

Fig. 3(a)–(d) demonstrate that Ge is present on the surface of the annealed sample C, while the bottom layer consists of Al and Ge. The strong Ge signals in Fig. 3(e) and (h) are likely attributed to these Ge/Ge structures corresponding to low-quality hillocks, formed on the sample surface in normal AIC.[11,13,27] Fig. 3(a)–(d) also demonstrate an AlO_x diffusion-limiting layer remained between the top and bottom layers, suggesting that the formative mechanisms of the top and bottom Ge are completely different. Fig. 3(e) shows the formative mechanism of the hillocks. First, Ge atoms diffuse into Al through the interlayer during annealing. When the Ge concentration in Al is supersaturated, Ge nucleation occurs.[12] The Ge crystals grow laterally due to the continuous supply of Ge atoms, and then push Al down to the bottom a-Ge layer,[13] making an eutectic system consisting of Al and Ge. In the eutectic system, Ge crystals precipitate with exhaling Al, resulting in the Ge hillocks formed on the bottom layer. Suppressing hillocks in the bottom layer, i.e., fabricating a uniform Ge on the surface is an advantage of inverted-AIC over normal-AIC.[27]

Now, the difference of the surface morphology between samples B and C is discussed from the perspective of the hillock formation. The cracks in sample B correspond to Al between Ge islands as shown in Fig. 2(d)–(f), meaning the insufficient coverage of the top Ge. Previously we found that GeO_x is weaker than AlO_x in terms of a diffusion barrier layer.[29] As seen in Fig. 2(e), sample B has relatively the large number of bottom hillocks compared to sample C. Considering the formative mechanism of hillocks presented in Fig. 3(e), the high incidence of hillocks in sample B is likely owing to the fast Al diffusion to Ge. Thus, this reduced the volume of the top Ge layer, resulting in the insufficient coverage of the top Ge layer in sample B.

The crystal quality of the samples after annealing was evaluated by using Raman spectroscopy and a θ-2θ XRD measurement. Before measurements, the surface Al layer of sample A was removed by using a diluted HF solution (1.5% HF). The Raman spectra in Fig. 4(a) show the peaks near 290 cm^{-1} for all samples. These peaks, especially the peak in sample B, shift to lower wavenumbers compared to the actual Ge optical phonon peak (300 cm^{-1}).[5] Although these large wavenumber shifts are not completely understood, presence of these peaks warrants the crystallization of Ge.

The θ-2θ XRD patterns in Fig. 4(b) show peaks at 27.2° for all samples, corresponding to the (111) plane in relaxed Ge, while other peaks do not appear. Considering the peak intensity ratio in Ge powder diffraction patterns (JCPDS 04-0545), the large XRD peaks in samples A and C indicate the preferential (111) orientation of Ge. In contrast, the weak XRD peak in samples B suggests the non-orientation and/or low crystallinity of Ge, which is consistent with the relatively broad peak in the Raman spectra of sample B shown in Fig. 4(a).

Using EBSD measurement, we characterized the detailed crystal orientation and the grain size of Ge for samples A–C. Fig. 5 shows the EBSD images in the normal direction (ND) and the transverse direction (TD) to the sample surface. For sample A, Fig. 5(a) and (b) indicate that small-grained, randomly-oriented Ge hillocks are scattered on a large-grained, (111)-oriented bottom-Ge layer. For sample B, Fig. 5(c) and (d) obtained at a Ge island, indicate submicron Ge grains with nearly random orientation. In contrast, for sample C, Fig. 5(e) and (f) indicate the highly (111) orientation and large grains in Ge. By using EBSD analysis, the (111) orientation fraction was calculated to be 96%, and the average grain size nearly 20 μm for sample C. In the normal AIC structure, the sample with GeO_x interlayer provided faster growth and smaller grain size compared to the sample with AlO_x interlayer.[29] The previous result is consistent with the present study on inverted AIC. The significant difference of the crystal orientation and grain size between samples B and C is attributed to the difference of Ge diffusion rates in the interlayers. The diffusion coefficient of Ge in AlO_x is two orders lower than that in GeO_x,[29] accounting for the different crystallization times between sample B (1 h) and sample C (15 h). We consider that the slow annealing induced Ge nucleation under thermal equilibrium conditions, resulting

in the energetically stable (111) plane pronounced in sample C.[14,26,35] Employing AlO_x interlayer limits the diffusion of Ge to Al, and thus allows for fabricating the highly (111)-oriented Ge layer.

Fig. 6(a) shows a representative cross-sectional bright-field TEM image of sample C, indicating the stacking structure of crystalline Al and Ge containing no obvious defects. Such a low-defect Ge is likely owing to the slow growth providing thermal equilibrium conditions. High resolution TEM image in Fig. 6(b) and a fast Fourier transform (FFT) analysis of the image in Fig. 6(c) demonstrate amorphous AlO_x remaining on the interface between crystalline Al and Ge layers. This result proves that the AlO_x membrane just works as a diffusion barrier; there is no epitaxial relationship between Ge and AlO_x. Fig. 6(d) shows a grain boundary observed in the upper Ge layer, likely attributed to the collision between lateral growth fronts. Some planar defects in Ge {111} planes such twin boundaries (TBs) and stacking faults (SFs) as shown in Fig. 6(e) and (f) were observed in the upper Ge layer. The lattice structure shown in Fig. 6(f), consisting of the large number of stacking faults, is not observed for poly-Ge formed by the solid-phase crystallization of a-Ge.[7] According to Huang *et al.*, the lattice structure possibly has a causal relationship with the formation of Al-Ge-O alloy during growth.[36,37] Note that these planar defects are almost parallel to the substrate owing to the (111) orientation of Ge. Thus, the resulting Ge layer will be useful for an epitaxial template for fabricating low-defect semiconductor layers.

Conclusions

We achieved the self-organization of Ge on conducting layer coated glass substrates utilizing the layer exchange in AIC at a low temperature of 325 °C. Controlling the interlayer between Al and Ge, i.e., limiting the diffusion of Ge to Al, significantly influenced the resulting structures: employing AlO_x interlayer led to the uniform Ge layer with highly (111) orientation (96%) and large grains (~20 μm). The resulting structure holds promise for use as buffer layers for the epitaxial growth of Ge, as well as of group III–V compound semiconductors, nanowires, and other advanced materials.

Acknowledgements

This work was financially supported by the Japan Science Society and the Iwatani Naoji Foundation. The authors are grateful to Dr. N. Fukata of NIMS for assistance in Raman measurement. Some experiments were conducted at the International Center for Young Scientists in NIMS.

Notes and references

[a] Institute of Applied Physics, University of Tsukuba, Tsukuba, Ibaraki 305-8573, Japan.
[b] Electron Microscope Facility, TIA, AIST, 16-1 Onogawa, Tsukuba 305-8569, Japan.

1 J. Michel, J. Liu and L. C. Kimerling, *Nature Photon*., 2010, **4**, 527.
2 R.R. King, D.C. Law, K.M. Edmondson, C.M. Fetzer, G.S. Kinsey, H. Yoon, R.A. Sherif and N.H. Karam, *Appl. Phys. Lett*., 2007, **90**, 183516.
3 R.R. Lieten, S. Degroote, K. Cheng, M. Leys, M. Kuijk and G. Borghs, *Appl. Phys. Lett*. 2006, **89**, 252118.
4 M. Suzuno, T. Koizumi, H. Kawakami and T. Suemasu, *Jpn. J. Appl. Phys*., 2010, **49**, 04DP05.
5 N. Fukata, K. Sato, M. Mitome, Y. Bando, T. Sekiguchi, M. Kirkham, J. I. Hong, Z. L. Wang and R. L. Snyder, *ACS Nano*, 2010, **4**, 3807.
6 M.G. Mauk, J.R. Balliet and B.W. Feyock, *J. Cryst. Growth*, 2003, **250**, 50.
7 K. Toko, I. Nakao, T. Sadoh, T. Noguchi and M. Miyao, *Solid-State Electron*., 2009, **53**, 1159.
8 C.Y. Tsao, J.W. Weber, P. Campbell, P.I. Widenborg, D. Song and M.A. Green, *Appl. Surf. Sci.*, 2009, **255**, 7028.
9 M. Tada, J.H. Park, J.R. Jain and K.C. Saraswat, *J. Electrochem. Soc*., 2009, **156**, D23.
10 O. Nast, T. Puzzer, L.M. Koschier, A.B. Sproul and S.R. Wenham, *Appl. Phys. Lett*., 1998, **73**, 3214.
11 Y. Sugimoto, N. Takata, T. Hirota, K. Ikeda, F. Yoshida, H. Nakashima and H. Nakashima, *Jpn. J. Appl. Phys.*, 2005, **44**, 4770.
12 A. Sarikov, J. Schneider, J. Berghold, M. Muske, I. Sieber, S. Gall and W. Fuhs, *J. Appl. Phys*., 2010, **107**, 114318.
13 B.I. Birajdar, T. Antesberger, B. Butz, M. Stutzmann and E. Spiecker, *Scripta Materialia*, 2012, **66**, 550.
14 M. Kurosawa, N. Kawabata, T. Sadoh and M. Miyao, *Appl. Phys. Lett.*, 2009, **95**, 132103.
15 I. Gordon, L. Carnel, D. Van Gestel, G. Beaucarne and J. Poortmans, *Thin Solid Films*, 2008, **516**, 6984.
16 S. Y. Wei, S. M. Yu, L. C. Yu, W. C. Sun, C. K. Hsieh, T. S. Lin, C. H. Tsai and F. R. Chen, *Cryst. Eng. Comm.*, 2011, **14**, 4967.
17 F. Katsuki, K. Hanafusa, M. Yonemura, T. Koyama and M. Doi, *J. Appl. Phys.*, 2001, **89**, 4643.
18 R. Zanatta and I. Chambouleyron, *J. Appl. Phys.*, 2005, **97**, 094914.
19 Z. M. Wang, J. Y. Wang, L. P. H. Jeurgens, F. Phillipp and E. Mittemeijer, *Acta. Materialia*, 2008, **56**, 5047.
20 S. Hu, A.F. Marshall and P.C. McIntyre, *Appl. Phys. Lett.*, 2010, **97**, 082104.
21 W. Zhang, F. Ma, T. Zhang and K. Xu, *Thin Solid Films*, 2011, **520**, 708.
22 S. Peng, D. Hu and D. He, *Appl. Surf. Sci*., 2012, **258**, 6003.
23 Q. Chen, C. Li, Z. Chen, Z. Jial, M. Wu, C. Shek, C. M. L. Wu and J. K. L. Lai, *Inorg. Chem.*, 2012, **51**, 8473.
24 M. Kurosawa, N. Kawabata, T. Sadoh and M. Miyao, *ECS J. Solid State Sci. and Tech.*, 2012, **1**, 144.
25 J.-H. Park, T. Suzuki, M. Kurosawa, M. Miyao and T. Sadoh, *Appl. Phys. Lett.*, 2013, **103**, 082102.
26 K. Toko, M. Kurosawa, N. Saitoh, N. Yoshizawa, N. Usami, M. Miyao and T. Suemasu, *Appl. Phys. Lett.*, 2012, **101**, 072106.
27 K. Toko, K. Nakazawa, N. Saitoh, N. Yoshizawa, N. Usami and T. Suemasu, *Cryst. Growth Des*., 2013, **13**, 3908.
28 R. Numata, K. Toko, K. Nakazawa, N. Usami, and T. Suemasu, *Thin Solid Films*, 2014, **557**, 143.
29 K. Toko, R. Numata, N. Oya, N. Fukata, N. Usami and T. Suemasu, *Appl. Phys. Lett*., 2014, **104**, 022106.

30 H. Kuraseko, N. Orita, H. Koaizawa and M. Kondo, *Appl. Phys. Express*, 2009, **2**, 015501.
31 C. Jaeger, M. Bator, S. Matich, and M. Stutzmann, *J. Appl. Phys.*, 2010, **108**, 113513.
32 M. Takeuchi and M. Kondo, *Jpn. J. Appl. Phys.*, 2014, **53**, 050303.
33 K. Toko, R. Numata, N. Saitoh, N. Yoshizawa, N. Usami and T. Suemasu, *J. Appl. Phys*., 2014, **115**, 094301.
34 S. K. Sahari, H. Murakami, T. Fujioka, T. Bando, A. Ohta, K. Makihara, S. Higashi, and S. Miyazaki, *Jpn. J. Appl. Phys.*, 2011, **50**, 04DA12.
35 A.A. Stekolnikov, J. Furthmüller and F. Bechstedt, *Physical Review B*, 2002, **65**, 1.
36 X. Huang, J. L. Coffer, J. A. Paramo, and Y. M. Strzhemechny, *Cryst. Growth Des.*, 2010, **10**, 32.
37 X. Huang and J. L. Coffer, *J. Phys. Chem. C*, 2010, **114**, 22019.

Table I. Sample structures before annealing.

Sample	Top layer (thickness)	Bottom layer (thickness)	Interlayer (air exposure time)
A	Ge (60 nm)	Al (50 nm)	AlO_x (10 min)
B	Al (50 nm)	Ge (60 nm)	GeO_x (24 h)
C	Al (50 nm)	Ge (60 nm)	AlO_x (10 min)

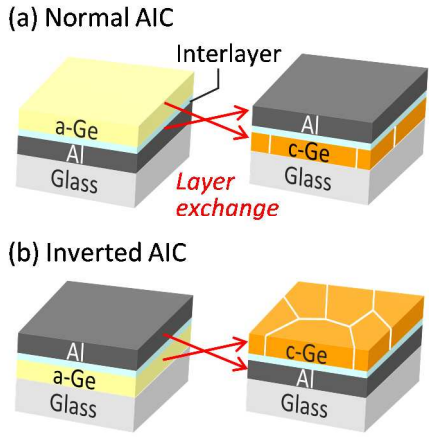

Fig. 1. Schematics of the sample structures: (a) normal-AIC (sample A) and (b) inverted-AIC (samples B and C) of a-Ge. The Interlayers between Al and Ge are AlO_x or GeO_x, working as diffusion limiting layers.

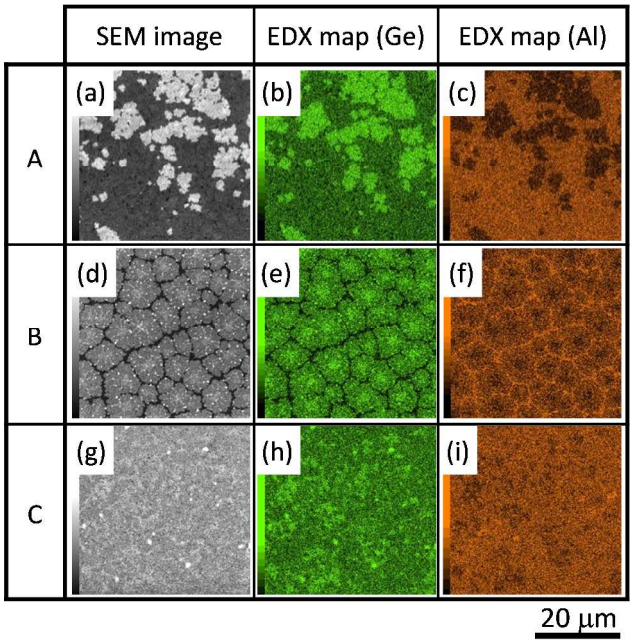

Fig. 2. Surface images and elemental maps of Ge and Al for annealed samples: (a–c) sample A, (d–f) sample B, and (g–i) sample C. The surface images were obtained by SEM, and elemental maps by EDX.

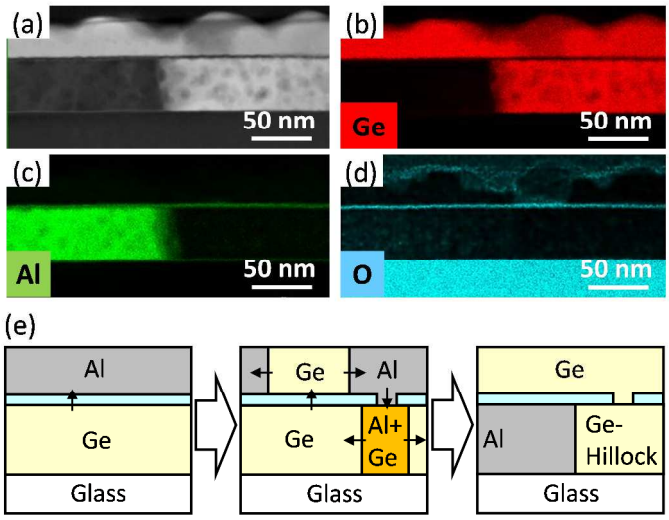

Fig. 3. Cross-sectional STEM-EDX analysis of sample C after annealing. (a) STEM-HAADF image. (b–d) Elemental maps of (b) Ge, (c) Al, and (d) O corresponding to the region shown in (a). (e) Schematic of layer exchange and Ge hillock formation during inverted AIC.

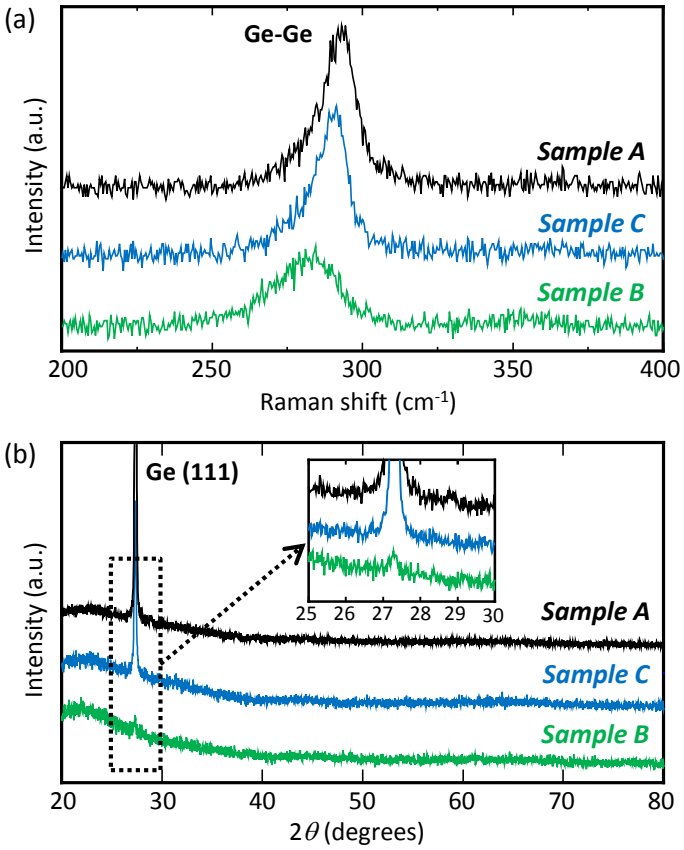

Fig. 4. (a) Raman scattering spectra obtained at the Ge regions in samples A–C after annealing. (b) ϑ–2ϑ XRD patterns of samples A–C after annealing. The insertion shows magnified patterns around Ge (111) peaks (~27.2°).

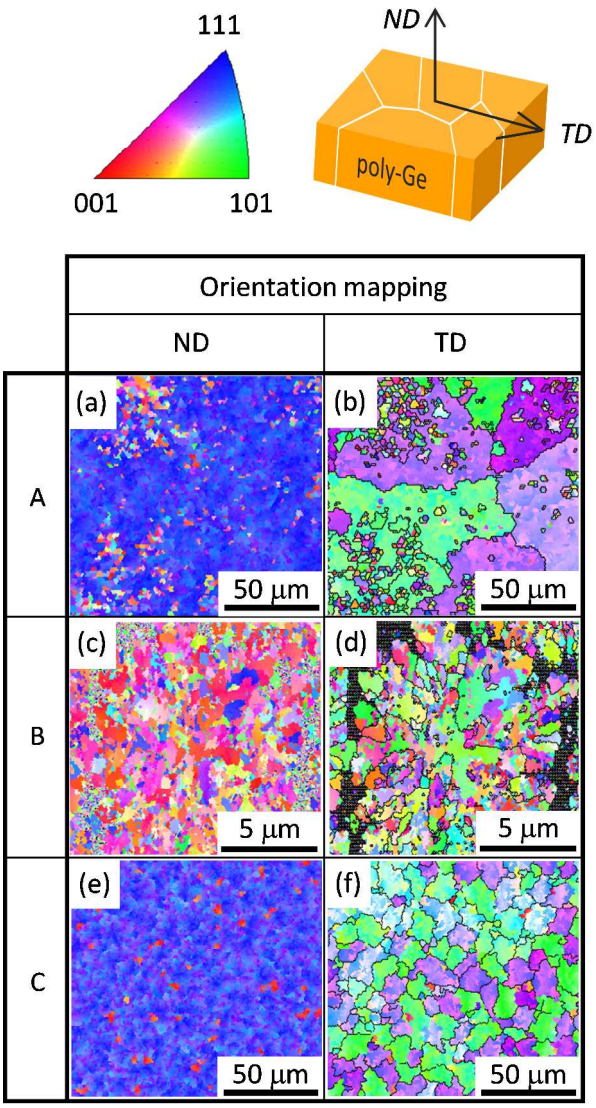

Fig. 5. EBSD patterns in ND and TD of the Ge layers for samples (a,b) A, (c,d) B, and (e,f) C. The ND and TD maps correspond to the same region. Coloration indicates crystal orientation, according to the legend. Black solid lines in the TD maps correspond to random grain boundaries.

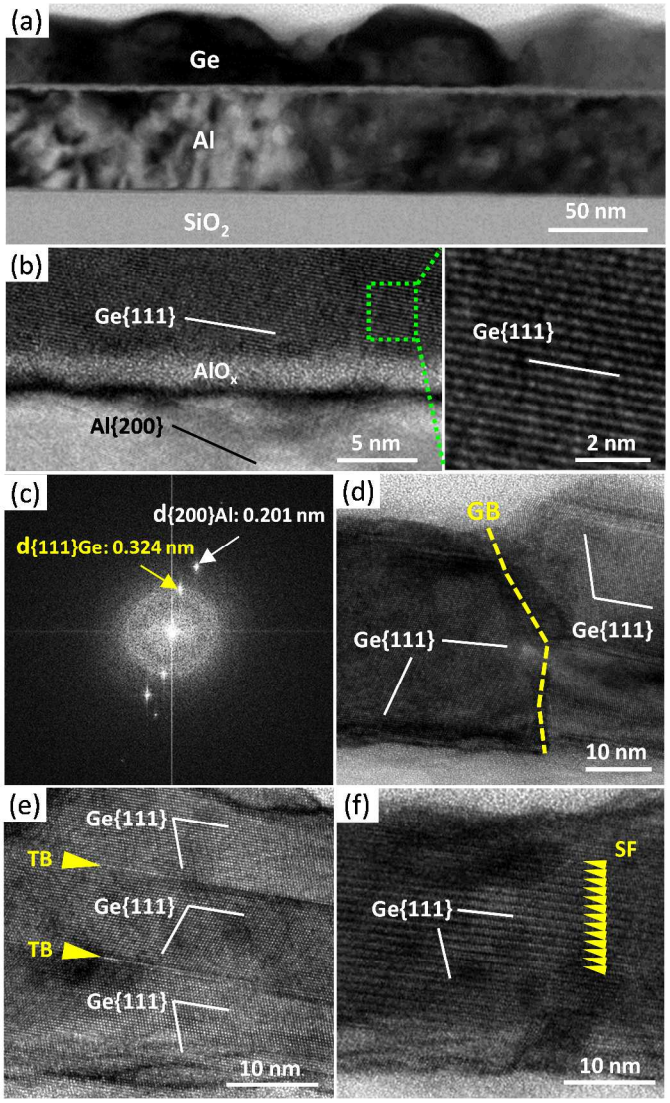

Fig. 6. Cross-sectional TEM images of sample C after annealing. (a) Representative bright-field image showing the stacking structure of large-grained Ge and Al. (b) High resolution image of the interlayer between crystalline Al and Ge layers with the magnified lattice image of Ge. (c) FFT pattern of (b). (d) High resolution image of a grain boundary in the Ge layer. (e,f) High resolution image of Ge{111} planar defects such as (e) TBs and (f) SFs. The white and black bars in the images indicate crystal planes.

Table of Contents Use

Self-organizing Ge(111)/Al/glass structures through layer exchange in metal-induced crystallization

Kaoru Toko,* Koki Nakazawa, Noriyuki Saitoh, Noriko Yoshizawa, Takashi Suemasu

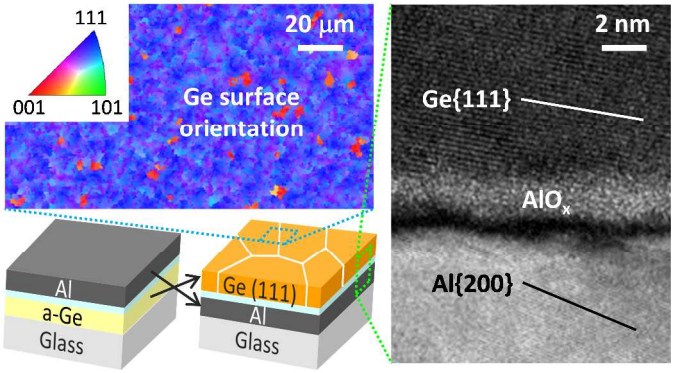

Al-induced crystallization enabled the self-organization of high-quality Ge/Al/glass structures through layer exchange at a low temperature of 325 °C.